

# Microextrusion Based 3D Printing – A Review

Edidiong Nseowo Udofia\*, Wenchao Zhou\*

*\*The AM<sub>3</sub> Lab, Department of Mechanical Engineering, University of Arkansas at Fayetteville  
Fayetteville, AR, United States of America; email: [zhouw@uark.edu](mailto:zhouw@uark.edu)*

---

## Abstract

Whilst extrusion-based 3D printing processes have been successfully applied at the macroscale, this seeming simplicity belies the dynamic complexities needed for consistent, repeatable and cost-effective printing at the microscale. To fully tap into the promise of microextrusion ( $\mu$ EP) of fabricating fine resolution features, it is critical to establish an understanding of the fundamentals of ink flow, interface energy, drying, and the process-property relationship of the printing process. Till date, a comprehensive and coherent organization of this knowledge from relevant literature in different fields is still lacking. In this paper, we present a framework of the underlying principles of the microextrusion process, offering an overall roadmap to guide successful printing based on both results in the literature and our own experimental tests. The impacts of various process parameters on the resolution of printed features are identified. Experiments are carried out to validate the developed framework. Key challenges and future directions of microextrusion 3D printing are also highlighted.

Keywords: Microextrusion, 3D printing, evaporation timescale, capillary rise, standoff distance, substrate driven ink flow, surface energy, PDMS printing

---

## I. INTRODUCTION

### 1.1. Background and Motivation

Three dimensional (3D) printing has emerged as a relevant manufacturing technology, with the potential to revolutionize the microfabrication industry [1-5]. Microextrusion-based 3D printing ( $\mu$ E-3DP) stands out as a promising alternative for microfabrication with a broad range of applications in biomedical [1, 6, 7], self-healing [8], sensors [9, 10], microfluidics [2, 11], and microelectronics[12-14] devices. As opposed to the classical manufacturing techniques, the attractions lie in the greater design freedom, fewer processing steps, lower cost for small production quantity, and a variety of compatible substrates. While this technique has been successfully applied for fabricating macroscale structures, this seeming simplicity belies the dynamic complexities needed for consistent, repeatable and cost-effective printing at the microscale. Another nascent area of  $\mu$ EP is extending the range of applicable materials, particularly materials with low viscosity and low surface energies; but the fundamental understanding that may enhance their applicability is still lacking. Here, our motivation is to develop a framework to provide an overall understanding needed for adapting microextrusion printing for microfabrication.

### Glossary of Symbols Used in this Paper

A	Cross sectional area of filament	$t_{\text{evap}}$	Evaporation timescale
c	Vapor concentration	$t_{\text{flow}}$	Flow timescale
Ca	Capillary number	u	Translating speed of the substrate
D	Nozzle diameter	v	Ink flow velocity
$D_i$	Nozzle inlet diameter	V	Ink volume
$D_t$	Nozzle tip diameter	$We$	Webber number
h	Standoff distance	$\gamma$	Shear rate
$h_c$	Critical standoff distance	$\mu$	Ink viscosity
I	Evaporation rate	$\rho$	Fluid density
J	Vapor diffusivity	$\sigma$	Surface tension
L	Nozzle length	$\sigma_e$	Surface energy
m	Mass of ink	$\sigma_{sv}$	Surface energy between substrate & vapor
p	Externally applied pressure	$\sigma_{sl}$	Surface energy between substrate & ink
$P_c$	Capillary pressure	$\sigma_{iv}$	Surface energy between ink & vapor
$P_s$	Surface tension pressure	$\theta$	Contact angle
Q	Flow rate	$\theta_a$	Advancing contact angle
$r_d$	Droplet radius	$\theta_e$	Equilibrium contact angle
R	Nozzle radius	$\theta_r$	Receding contact
Re	Reynolds number	$\tau$	Shear stress
t	Time		

## 1.2. Overview of Microextrusion

Microextrusion 3D printing describes a layer-wise (additive) manufacturing method where parts are built from bottom-up to create arbitrary 3D features, and the resulting feature has at least one of its dimensions in the micrometer range [15]. In Figure 1 we illustrate the overview of the microextrusion printing. It involves the arrangement of a material dispensing system with a pneumatic or mechanical (piston or screw) drive and a computer-controlled robotic platform for extrusion and deposition onto a substrate. It usually produces continuous filaments and is distinguished from other digital writing technologies, such as inkjet [16] and electrohydrodynamic jet (ejet) printing [17], which are droplet-based processes. This strategy is maskless, cost-effective, with a wide range of material choice, and high-resolution printing capability [18].

The design freedom availed by  $\mu$ EP opens new design possibilities and local material property modulation. Till date, this approach has been applied to print a variety of materials including colloidal gels [19, 20], fugitive gel [21], biocompatible [22-27] and polymer-based inks [28-30]. For example, Lewis et al. demonstrated omnidirectional printing of flexible, stretchable, and spanning silver microelectrodes [12]. Dermanaki-Farahani et al.[31] used a combination of nanoparticle infiltration and microextrusion printing to fabricate functionally graded structural beams with tailored local properties. Printing of functional devices, e.g., batteries [32-34], electronic components (e.g., transistors) [35-38], biomedical [39] and microfluidic devices [40-42], and smart materials [43, 44] are also reported. Ideally, inks for  $\mu$ EP must exhibit a pseudoplastic (or shear thinning) and viscoelastic properties to facilitate production of fine

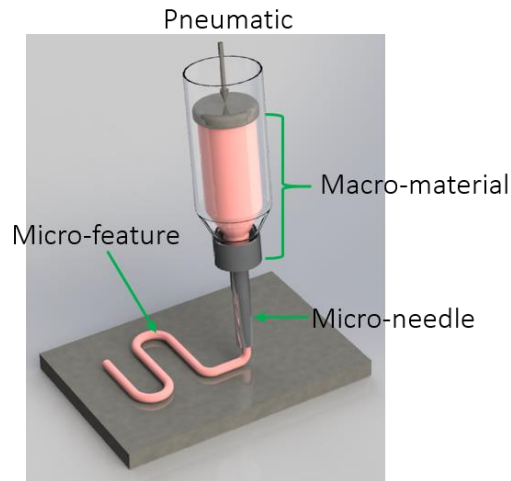


**Figure 1: Schematic illustration of microextrusion printing**

ink filament that rapidly solidifies upon deposition to facilitate shape retention [45]. However, this requirement constrains the range of usable materials. It often demands careful control of ink rheology, dynamics of fluid flow and deposition, and characteristics of shape retention on the substrate. The driving forces of the ink flow at the microscale are expected to be largely different from those at the macroscale.

To make a successful print, generally, the literature report two primary paths: (1) design of new ink with requisite properties [45], and (2) the development of empirical models that quantify the effect of the various process parameters on the resolution of printed features [46-48]. For example, Lewis and coworkers have developed several inks, and have successfully printed features with a millimeter to a few micron resolutions [21, 37, 49, 50]. Darta reported quantification of the effects of ink rheology and printing parameters on the resolution of printed features [46]. Besides these, other researchers have also reported models for predicting prints resolution and quantifying the effects of various process parameters, such as extrusion pressure, nozzle size, substrate type and velocity, and standoff distance [22, 51-53]. Nevertheless, these approaches have not addressed the fundamental theoretical foundations that may enhance effective understanding of the  $\mu$ EP process. There is a high demand for high-resolution printing of traditionally low viscous materials, but this is yet to be fully realized [28, 54].

### 1.3. Paper Overview

The interests in adapting microextrusion for different applications spurs the need to fully investigate and answer some of the fundamental questions: (1) *what are the ink properties that determine printability, and shape retention characteristics?* (2) *what are the dominant driving forces that govern ink extrusion at the microscale?* (3) *what are the major factors that determine the final resolution of printed filament?* (4) *how do we modulate these factors to meet the requirements of target applications?* The ability to understand and answer these questions will determine if one can perform a successful  $\mu$ EP or not.

Our goal in this paper is to answer these questions, which we approach on two fronts. First, to tackle the lack of fundamental understanding of this printing technique, in section II, we present a roadmap for successful printing –providing an overarching perspective into the critical parameters affecting the printing process. A guide to controlling each parameter, employing both numerical and experimental techniques to understand the process is offered. Second, in section III, we validate the applicability of the framework by printing high-resolution features using Polydimethylsiloxane (PDMS) ink. Finally, aided by this knowledge, challenges and future direction of microextrusion are discussed in section IV.

## II. ROADMAP FOR SUCCESSFUL MICROEXTRUSION PRINTING

The factors influencing  $\mu$ EP are numerous and interrelated. Extruded ink filaments undergo varying static and dynamic phenomena, which bear significant influence on the printing resolution. For instance, the dynamics of the ink that has been deposited on the substrate is very different from the dynamics of the flowing ink at the nozzle tip. To understand the whole process, four phases of microextrusion printing have been identified (Figure 2) and will be discussed in this section:

- a) Phase 1: Flow prediction inside the nozzle;
- b) Phase 2: Extrusion from the nozzle tip;
- c) Phase 3: Deposition onto a moving substrate;
- d) Phase 4: Time-dependent wetting.

The feature resolution (i.e., width (W), and thickness (H) of the deposited filament area) can be expressed as a function of surface property (e.g., contact angle  $\theta$ ), printing speed (u), standoff distance (h) and flow rate(Q) (Eq.1). Flow rate is a function of several variables, including pressure (P), ink viscosity ( $\mu$ ), nozzle diameter (D), nozzle length (L) and surface tension ( $\sigma$ ).

$$(\text{Width, Height}) \sim f(Q, u, \theta) = f(Q(P, \mu, L, \sigma, h, D), u, \theta) \quad (1)$$

The typical range of the process parameters reported in the literature and their relationships to the feature resolution are summarized in Table 1, which shows how each input variable (e.g., printing speed, standoff distance, nozzle size), affects the printing process. Subject to the application, control over feature thickness may be desired at the expense of width and vice versa. For instance, if the desire is to print thin films, then control over layer thickness takes the priority.

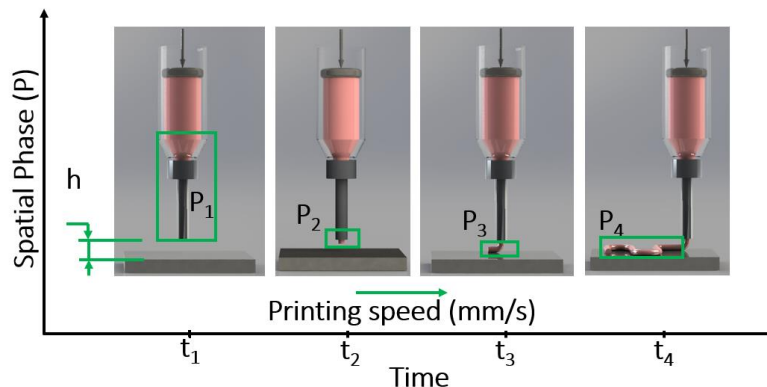


**Figure 2: Schematic of printing dynamics in different phases (i.e., space and time)**

**Table 1: A summary of important parametric relationships**

Variable	Typical Range		Underlying Relationships
Nozzle size	[~0.1 - 250 $\mu\text{m}$ ]	1	Feature resolution is directly proportional to the nozzle size.
Surface property	[ $0^\circ \leq \theta \leq 180^\circ$ ] With $90^\circ$ considered as optimum [55]	1	Substrates with low surface energy prevent surface wetting and ink spreading.
		2	High surface energy nozzles and substrates result in a high degree of capillary rise and excessive spreading of printed filament respectively.
		3	The lower the contact angle, the higher the spreading.
Surface tension	11.91- 72.80mN/m [56]	1	As the printing scale goes down, the effect of surface tension increases, and provides additional resistance to ink flow.
Viscosity	1127 – 1.3x 10 <sup>9</sup> cP [21, 53]	1	High viscosity materials require high pressures which make it difficult to extrude through very fine nozzles.
		2	Low viscosity materials flow easily but are plagued with surface wetting issues.
Printing speed	[0.1-5mm/s]	1	Relative to the flow rate, a low printing speed results in more ink being deposited per unit time which culminates in poor lateral resolution.
		2	A high printing speed leads to fine features but if not matched with appropriate flow rate can lead to discontinuous filaments.
Deposition Pressure	[0.5-100psi]	1	The flow rate is proportional to the applied pressure. Increased pressure translates to increased flow rate.
		2	Excessive pressure could damage ink reservoirs or microneedles and presents safety concerns, which sets an operational limit on the applicable pressure [57].
Standoff Distance	[~ size of the nozzle tip]	1	The standoff distance refers to the distance between the nozzle tip and the substrate or the preceding deposited filament layer. As the printing scale goes down (and by effect the standoff distance), flow rate becomes sensitive to the standoff distance. Flow rate decreases as standoff distance decreases [58].
		2	At high standoff distance (about 3 times the size of the nozzle diameter), the excess gap can lead to filament breakup due to the interaction of inertial and surface forces[59].

## 2.1. Phase 1: (P1) Flow Prediction Inside the nozzle

In phase 1, ink is flowing inside the nozzle under external pressure. An optimal control of ink rheology and extrusion rate are essential to achieving continuous and fine prints resolution. The ink extrusion rate is influenced by three primary factors including material properties, nozzle geometry and other user-imposed conditions such as temperature (Figure 3a). In order to examine these factors and how they may be optimized, in section 2.1.1 we present the various types of ink flow behavior, effect of nozzle geometry is discussed in section 2.1.2, while some key flow predictive models are presented in section 2.1.3.

### 2.1.1. Rheological Ink Properties for Microextrusion Printing

Rheology deals with the study of deformation and flow of “fluidic matter” under controlled shear conditions. During the dispensing process, inks are subjected to different deformation and transformational rates due either to the applied pressure, nozzle size, temperature or other processing conditions which influence their final shape or cell survival (for biological constructs). Rheological characterization provides a means of measuring such changes (e.g., viscosity) since stability, ease of flow, and self-supportability can be directly correlated to the observed behaviors

[51, 60-63]. The suitability of a material for  $\mu$ EP is governed by two important criteria: (1) ability to flow easily through fine needles upon application of force, and (2) set immediately after deposition to enable the creation of stable and high-fidelity structures. Figure 3b illustrates the different types of flow responses under steady shear.

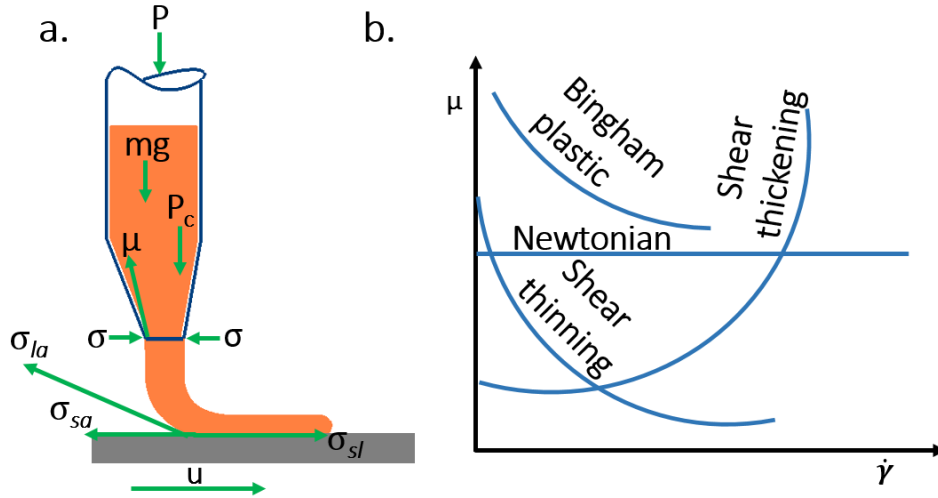


**Figure 3: (a) Schematic illustration of the dynamics of microextrusion deposition process - applied pressure; the weight of the ink in the syringe ( $mg$ ); capillary pressure ( $P_c$ ); surface tension ( $\sigma$ );  $\sigma_{sa}$ ,  $\sigma_{sl}$ , and  $\sigma_{la}$  are the interfacial energy interactions between substrate and air, the substrate and ink, and ink and air respectively; as well as the translating speed of the substrate ( $u$ ), (b) Flow behaviors exhibited by different ink designs**

The simplest case describes a Newtonian flow behavior, where viscosity is independent of shear rate. This ink type is typical of low-viscosity, prone to surface wetting, lacking self-supportability, and therefore not suitable for  $\mu$ EP. The remaining three are categorized as non-Newtonian materials, in which viscosity depends on the shear rate. The shear thinning behavior is characterized by a decrease of viscosity as shear rate increases and is considered the ideal for  $\mu$ EP, because this decrease in viscosity facilitates flow through nozzles, and rapidly increases upon deposition to enable shape retention [45]. On the other hand, the shear thickening behavior is characterized by an increase of viscosity as shear rate increases, possessing self-supportability, but the requirement of high pressure needed to sustain flow makes it unsuitable for  $\mu$ EP. The Bingham plastics often require a certain shear force (yield stress) to be applied before flow begins, and until this stress value is reached they behave much like solids. In general, material viscosity ( $\mu$ ) may be related to the applied shear stress ( $\tau$ ) and shear rate ( $\dot{\gamma}$ ) by [64, 65]:

$$\tau = \mu \dot{\gamma}^n \quad (2)$$

where  $n$  is the flow index (for Newtonian inks,  $n = 1$ ). There are other aspects of ink formulation (e.g., interparticle bonds, PH value, nozzle-to-particles ratio needed to prevent clogging) that are equally important but beyond the scope of this paper; nonetheless, there are already many excellent reviews on these subjects[19, 20, 45, 48, 66-68].

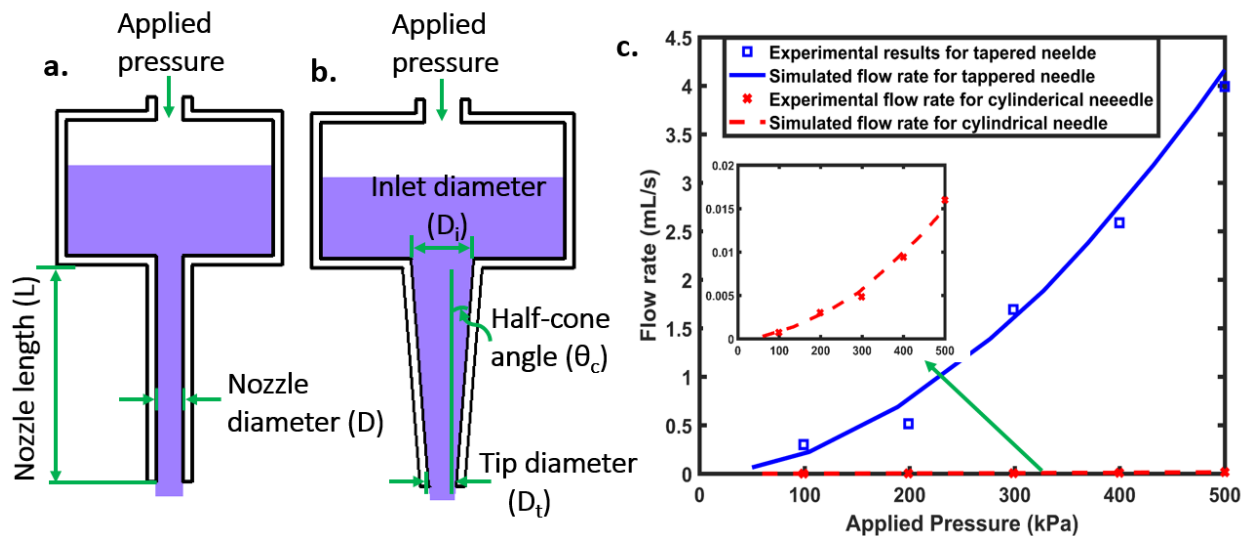


**Figure 4: Effect on nozzle geometry on flow rates. (a) Cylindrical nozzle, (b) Tapered nozzle. (c) Comparison of flow rate vs extrusion pressure for cylindrical and tapered needles. Embedded figures are enlargements of cylindrical needle data. Results for outlet diameter 0.25mm. (Redrawn based on [65]).**

### 2.1.2. Effect of Nozzle Geometry on Fluid Flow

The size and geometry of the dispensing nozzle dictate the flow rates (i.e., the quantity of ink filament leaving the nozzle tip per unit time), and therefore draws attention to the need of fine-tuning it to achieve optimal flows. As can be inferred from Figure 3a, there are three primary factors resisting ink flow inside the nozzle: (1) the nozzle geometry, (2) surface tension force, and (3) viscosity which describes ink's resistance to flow. The role of nozzle geometry will be discussed in this section.

There are two popular nozzle types, cylindrical and tapered nozzles (Figure 4a) identified in the literature. Results show that under similar operating conditions, the tapered nozzle triggers a higher-pressure gradient (and flow rate) than achievable from a cylindrical nozzle [65, 69]. Figure 4c shows the experimental and numerical results carried out by Li et al. to verify this influence, and what they found was that under identical conditions (e.g.,  $D=250\mu\text{m}$ ,  $P=500\text{kPa}$ ) the tapered needle triggered much higher flow rates ( $\sim 200$  times) than the cylindrical nozzle [65]. A reasonable explanation to this result is that tapered needles typically have larger diameters at the entrance, and a smaller diameter at the tip; a feature which provides a more favorable pressure gradient, dictated by the cone-half angle and tip diameter (Figure 4a) [69]. The quantitative effects of the cone-half angle will be discussed in section 2.1.3 (see Eq. (5)). Thus, in situations where the extrusion pressure is limited, a tapered nozzle will be the best option for achieving a higher flow rate, especially when dispensing high viscosity materials.

### 2.1.3. Models for Predicting Flow Rates

Taking the discussions in sections 2.1.1 and 2.1.2 together, several quantitative models have been proposed for estimating the flow rates. Here, we examine some of these models and offer a discussion on their applicability in predicting flow rates for  $\mu\text{EP}$ .

**Table 2: Typical ink flow rate for microextrusion printing**

Ink design	Viscosity (cP)	Nozzle diameter (μm)	Applied Pressure (kPa)	Flow rate	References
<b>Newtonian:</b>					
Deionized water	1.0	42	11.6-91.5	5.62-16.9uL/s	[53]
PLLA solution	1127	20	13.33-21.22	0.071-0.113nL/s	[69]
<b>Non-Newtonian</b>					
Polyelectrolyte ink	7600	0.5	170	0.00392pL/s	[70]
Sodium alginate solution	>2000	330	56.5-221	1.1-33.2uL/s	[65]
Cells suspension	10820	250	100-500	0.3-4.0mL/s	[71]
Petroleum jelly-wax (80/20)	8.4- 9.6x 10 <sup>5</sup>	510	210-290	0.15-0.81uL/s	[22]
Fugitive ink	*2.94x10 <sup>3</sup> -1.3x10 <sup>9</sup>	200	2.9MPa	-	[21]
Reported range	10 <sup>0</sup> – 1.3x 10 <sup>9</sup>	20-510	11.6kpa -2.9MPa	0.07nL/s-4mL/s	

\*computed at the shear rate of 400 and 8.21x10<sup>5</sup> respectively.

First, in Table 2, we provide a summary of the typical flow rates (which are in the range of μ-pL/s), applicable nozzle size, extrusion pressure, and viscosity. One trend is observed in this table, that is, the extrusion of highly viscosity materials through fine needles requires high pressures (i.e., pressure requirement increases with increase in viscosity or/ and a decrease in nozzle diameter). For the simple case of a Newtonian ink flowing through a cylindrical nozzle, the flow rate can be approximated by the Hagen–Poiseuille law [53]:

$$Q = \frac{\pi D^4 \Delta P}{128 \mu L} \quad (3)$$

Where ΔP is the pressure difference across the nozzle length (L), μ is dynamic ink viscosity, D is the nozzle diameter. Khalil & Sun developed a modified form of Eq. 3 to account for Non-Newtonian flow behaviors [22]:

$$Q = \left( \frac{n}{3n + 1} \right) \pi \gamma_o^{\frac{n-1}{n}} \left( \frac{\partial P / \partial z}{2 \mu_o} \right)^{1/n} R^{\frac{3n+1}{n}} \quad (4)$$

where R is the radius of the nozzle, μ<sub>o</sub> is the viscosity at a low shear rate, γ<sub>o</sub> is the shear rate, z is the direction of nozzle axis, n is the flow index, so that for Newtonian inks (where n =1), Eq. 4 reduces to Eq. 3. In contrast with equation 3 and 4 which are based on cylindrical nozzle assumptions, for a tapered nozzle geometry (Figure 4b), the flow rate may be described by [65]:

$$Q = \frac{\pi D_i^3 D_t^3}{32} \left[ \frac{3n \Delta P \tan \theta_c}{2 \mu (D_i^{3n} - D_t^{3n})} \right]^{1/n} \quad (5)$$

where D<sub>i</sub> and D<sub>t</sub> are the diameters of the nozzle entrance and exit respectively as marked in Figure 4(a). Clearly, the effect of the nozzle geometry (cone-half angle) and the flow rate is evident from

this equation. As revealed by Eq. 5, the larger the cone half-angle, and the smaller the flow index, the higher will be the flow rate.

In summary, the ink flow rate is: (i) inversely proportional to the viscosity ( $\mu$ ), (ii) directly proportional to the applied pressure ( $P$ ), (iii) inversely proportional to the pipe length ( $L$ ), and (iv) directly proportional to the nozzle diameter. The strong dependence of flow rate on nozzle diameter is apparent. For instance, based on Eq. 3, if the desire is to increase flow rate, then increasing the nozzle diameter by a factor of 2, with other parameters fixed, the flow rate increases by a factor of 16 (i.e.  $Q \sim D^4$ ).

## 2.2. Phase Two ( $P_2$ ): Extrusion from the Nozzle Tip

As the printing progresses to phase 2, there are many possible outcomes, including nozzle clogging, surface wetting, and a high degree of solvent evaporation. Our objective is to capture the underlying dynamics as the ink exits the nozzle into the air and interacts with the nozzle surface. This complex process will be discussed under two categories: capillary rise effect in section 2.2.1, and evaporative effect in section 2.2.2.

### 2.2.1. Capillary Rise Effect

Capillary rise refers to the upward rise of dispensed ink at the nozzle tip-air interface due primarily to the interplay between viscous and surface forces. There are two possible causes of this observation. First, pneumatic dispensing systems suffer from a time lag between when the “stop printing” process is initiated, and when material flow stops. This phenomenon can lead to material still oozing out and subsequent build-up at the nozzle tip during translation from point to point where material extrusion is not required and may, therefore, impede smooth dispensing and lower the print resolution. Second, capillary rise is driven by ink wettability at the nozzle tip, which describes the degree of affinity between a liquid and the nozzle surface (hydrophobic and hydrophilic surfaces) [72], and this tendency is increased if the nozzle surface is wetted/wettable [73], and if the ink is of low viscosity. Here, we examine instances where capillary rise could become a significant challenge, and tools that may be employed to control the process to achieve successful printing.

To obtain a quantitative estimate when capillary rise may be significant, the capillary number ( $Ca$ ), may be calculated to express the relative importance of the surface tension to viscous force:

$$Ca = \mu v / \sigma \quad (6)$$

As can be understood from this equation, the surface tension force tries to reduce surface area by maintaining a spherical shape, while the viscous force opposes any possible change in shape. A strong indication of capillary dominated flow occurs when  $Ca = 10^{-1} \sim 10^{-3}$ . Hence, as a rule of thumb, ***with ink of low viscosity and low surface energy, if the nozzle has a higher surface energy than the ink (see section 2.4. on surface energy) and  $Ca < 10^{-1}$  [74] then the ink may wet the nozzle surface, giving rise to high capillary effect.*** To validate this theory, extrusion of 100 wt.% glycerol is demonstrated (Figure 5). According to results by Chang et al. [73] and buttressed by our experimental results, at low flow velocity and low viscosity inks, the extrusion process is

marked by low capillary number ( $Q = 228 \text{ pL/s}$ ,  $v = 0.323 \text{ mm/s}$ ,  $Ca = 6.38 \times 10^{-3}$ ), and ink filament is pulled upward along the nozzle surface if surface energy of the nozzle is greater than that of the ink ( $\sigma_{e(\text{glass})} = 310 \text{ mN/m}$ ,  $\sigma_{e(\text{glycerol})} = 70.9 \text{ mN/m}$ ) (Figure 5b). Subsequently, the ink is observed to grow into a spherical shape which is about 9-fold greater than the nozzle diameter (Figure 5c). In contrast, as the capillary number increases, (i.e., by increasing the flow rate,  $Q = 3.91.8 \text{ nL/s}$ ,  $v = 5.54 \text{ mm/s}$ ,  $Ca = 1.09 \times 10^{-1}$ ), continuous ink filament is produced with a diameter equal to the nozzle diameter (Figure 5d).

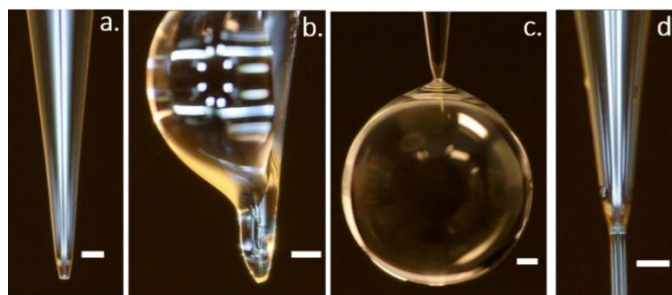


**Figure 5: Illustration of capillary rise effect using 100% glycerol with 30 $\mu\text{m}$  nozzle tip – (a) Unfilled nozzle tip, (b) At 7 psi extrusion pressure, capillary rise hinders formation of ink filament or droplet, (c) Droplet grows to  $\sim 9 \cdot D$  before pinching off, (d) At 120psi, continuous ink filament is produced, which is about the size of the nozzle tip. (Scale bars are 60 $\mu\text{m}$ ).**

In summary, capillary rise effect tends to cause material build-up at the nozzle tip and reduces print resolution. In the extreme cases of high evaporative effect (see the next section for discussion) partial clogging of the nozzle may be observed. In relation to the length scale, it is apparent that as the length scale goes down (if other factors are fixed) the tendency of capillary rise increases. To limit the effect of capillary rise, the literature reports the usage of high viscosity materials and nozzle surface coating [29, 75]. At different combinations of ink viscosity, flow velocity and surface tension Eq. 6 may be used to determine the appropriate working range.

### 2.2.2 Evaporative Effect

Evaporative effect describes the change in flow behaviors due to rapid solvent loss in the extruded ink filament at the periphery of the nozzle tip-air interface. Significant moisture loss can alter ink rheology, and flow rates by causing partial or complete ink solidification at the nozzle tip [49, 67, 76]. On the other hand, accelerated solvent loss (Figure 6a, due to the increased surface-area-to-volume ratio) have been employed for the creation of arbitrary free-standing structures [77, 78]. Under isothermal condition, the rate of solvent evaporation is enhanced by two primary factors: (1) the prevailing ambient condition (e.g., relative humidity), and (2) boiling point of the solvent (e.g., Isopropyl alcohol- boiling point 82.5 $^{\circ}\text{C}$ , water -boiling point 100 $^{\circ}\text{C}$ , ethylene glycol - boiling point 197.3 $^{\circ}\text{C}$ , and glycerol -boiling point 290 $^{\circ}\text{C}$ ) [3].

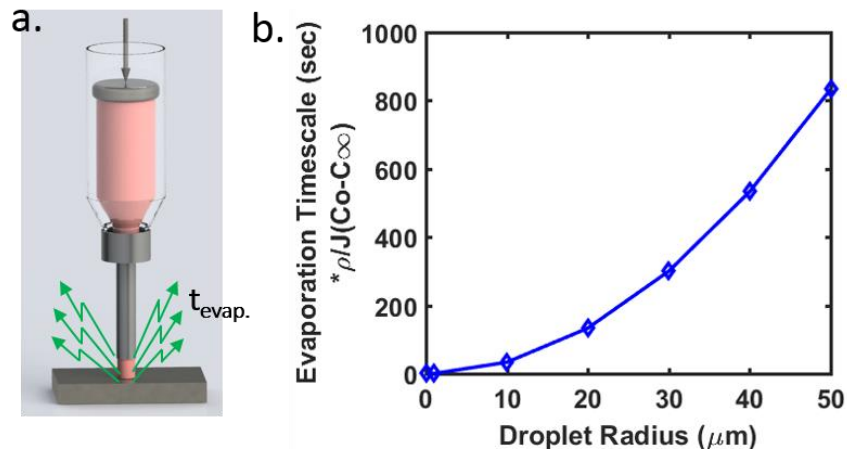


**Figure 6: (a) Illustration of solvent evaporation at the microscale, (b) Plot of evaporation time as a function of droplet radius**

To gain a perspective if the evaporative effect would pose a printing challenge, we propose to compare the drying time scale and the extrusion time scale. For instance, if the drying timescale is much smaller than the flow timescale, a large amount of solvent evaporates affecting ink extrusion. Conversely, if the drying timescale is very large compared to the flow timescale, very little moisture is lost before it flows out, and this effect becomes insignificant. To this end, we performed a quantitative analysis of evaporation and flow rates, to estimate their relative significance. For the simple case of a stationary spherical droplet of a pure liquid, the rate of evaporation into the ambient air may be expressed by the equation:

$$I = \frac{-dm}{dt} = -\rho \frac{dV}{dt} \quad (7)$$

where  $I$  is the evaporation rate with a unit of  $\text{g/s}$ ,  $m$  is the mass of drop,  $\rho$  is the density of the ink, and  $V$  is the volume of the drop. Birdi et al. [79, 80] expressed Fick's law for the rate of evaporation as follows:

$$I = -4\pi r^2 J \frac{dc}{dr} \quad (8)$$

Where  $J$  ( $\text{mm}^2/\text{s}$ ) is the diffusivity of the vapor and depends on the temperature, and  $c$  is the concentration of the vapor per unit volume of air ( $\text{g}/\text{mm}^3$ ). Applying the following the boundary conditions to Eq. 8 for a droplet at infinite distance ( $c = c_\infty$ , at  $r = \infty$ ;  $c = c_0$  at  $r = r_d$ , where  $r_d$  is the radius of the liquid drop), it is seen that the rate of evaporation is dependent on the diffusivity of the vapor and the droplet radius (Eq. 9) [79]:

$$I = 4\pi r_d J (c_0 - c_\infty) \quad (9)$$

By combining Eq. 7 and 9, the evaporation timescale is expressed as:

$$t_{evap.} = \frac{dV}{4\pi r_d J} \frac{\rho}{(c_o - c_\infty)} \quad (10)$$

While the flow timescale may be expressed as the ratio of nozzle radius (R) and the average extrusion velocity (v).

$$t_{flow} = \frac{R}{v} \quad (11)$$

Apparently, at a constant temperature and relative humidity, the volume-to-surface-area ratio ( $dV/4\pi r_d$ ) becomes the only variable in Eq. 10 and reveals that the evaporation timescale decreases with a decrease in droplet radius. Indeed, this is confirmed by the plot of ( $dV/4\pi r_d$ ) versus the droplet radius having a quadratic relationship between  $t_{evap.}$  and the nozzle size (Figure 6b). This observed correlation is attributed to the increased surface area which acts as a driving force to accelerate solvent loss. On the other hand, a linear relationship exists between the flow time and the droplet radius (Eq. 11). Therefore, for a given ink, if the filament geometry, flow rate, and diffusivity of solvent into ambient air are known, then evaporation and flow timescales can be calculated to estimate their relative effects.

For example, to compare these two timescales, we considered extrusion of water from a 30 $\mu$ m diameter nozzle and a flow rate of 0.358 $\mu$ L/s ( $v = 5.08 \times 10^{-4}$  mm/s). At 40% relative humidity, water vapor diffusivity  $J = 26.1$  mm<sup>2</sup>/s [81], the flow and evaporation timescales are 1.97s and 5220s respectively. The importance of this result is that under the stated conditions, flow happens ~2650 times faster than evaporation, and would therefore not affect printing significantly. On the hand, if printing was done using a 1 $\mu$ m nozzle and a flow rate of 0.443fL/s ( $v = 5.65 \times 10^{-7}$  mm/s) under the same conditions, the flow and evaporation timescales would be 1770s and 0.194s respectively. This means evaporation happens ~9123 times faster than flow and will, therefore, hinder successful printing. To limit high rate of evaporation, printing inside a non-wetting oil reservoir has been reported [49, 64]. Evidently, the need to overcome alterations in ink rheology and nozzle clogging arising from the rapid drying rate (at the microscale) presents several challenges to be overcome and hinders the drive to further improving the printing resolution. Some of these challenges include appropriate ink formulation [49, 64], and better control of the printing environment and innovative support materials formulation [82].

### 2.3. Phase 3 (P3): Kinetics of Deposition onto a Moving Substrate

In this phase, the ink filament makes the first contact with the translating substrate, and a plethora of experimental and numerical evidence from the literature demonstrate the critical influence of the substrate speed on the print resolution [19, 62]. However, such important question as *does the substrate translating speed drive ink flow from the nozzle?* have received little attention in the literature. For instance, at very low flow rates, the substrate speed exerts a dominant influence on the flow rate and may therefore drive ink flow. Here, we take the experimental route to demonstrate and answer this question which may open a new avenue for patterning features from very fine nozzles where the demand for high pressure may prove challenging. To effectively capture this observation, the discussion in this section will be divided into two sections: effect of standoff distance (section 2.3.1) and the effect of the translating substrate (section 2.3.2).

### 2.3.1. The Effect of Standoff Distance

The primary finding, which we now offer explanatory insights is that: if other parameters are held constant, decreasing the standoff distance to less than ~50% of the nozzle diameter leads to increased flow resistance. That is, by reducing the effective nozzle diameter, and generation of back pressure which results in a reduction of flow rate (Figure 7a) [19, 59, 83]. The need to reduce the standoff distance is a consequence of utilizing fine nozzles, in which case, the standoff distance must be finely tuned as well in order to produce continuous prints. On the other hand, at a high standoff distance (i.e.,  $h > \pi * D$ ) [59, 84] the ink filament can become unstable, leading to break up into discrete droplets due to the Plateau-Rayleigh instability [48], and poor adhesion to the substrate.

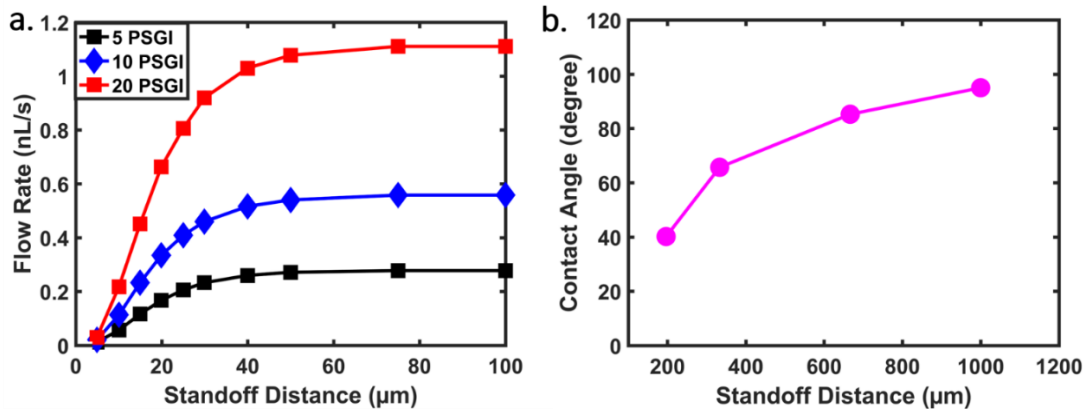


**Figure 7: Illustration of the effect of standoff distance: (a) On flow rate using 50μm nozzle tip (redrawn based on [58]), (b) On contact angle using 700μm nozzle tip (redrawn based on [19]).**

Through an empirical study, Wang and Shaw [19] showed that for a given set of flow rate( $Q$ ), nozzle diameter and printing speed ( $u$ ) there is a critical standoff distance ( $h_c$ ) that guarantees that just enough amount of material is available between the nozzle tip and the substrate expressed as:

$$h_c = \frac{Q}{uD} \quad (12)$$

For every ink-substrate pair, there is a specific contact angle if a critical standoff distance was maintained. However, if  $h < h_c$ , a compression effect will be induced and by effect altering the contact angle between the ink filament and substrate. Conversely, if  $h > h_c$  there will be enough space for the ink to occupy in which case, the contact angle is only controlled by ink rheology and surface energy (discussion in phase 4) of the substrate. By measuring the contact angle, Wang and Shaw [19] obtained a quantitative estimate of the degree of filament spreading due to low standoff distance. In their study, it was revealed that when standoff distance  $h$  is 670μm (which was near the critical value,  $h_c = 840\mu\text{m}$ ), no spreading was observed, and the equilibrium contact angle at this point is ~85° (Figure 7b). On the other hand, when the standoff distance was decreased from 670 to 335μm, the contact angle decreased from ~85° to 65.3° (~ 23.2% decrease). However, when the standoff distance was increased from 670 to 1000μm, very little change in contact angle was observed (~85 to 95.7°, ~12.6% increase).

The current barriers to improving printing resolution due to challenges of inappropriate standoff distance are summarized here and illustrated in Figure 8. For example, if the nozzle tip is too close

to the substrate, the nozzle can be damaged (Figure 8b), while large standoff gap results in discrete droplets (Figure 8c). Furthermore, a high standoff distance will increase the travel time of the filament through air relative to drying time, ink solidifies before reaching the substrate; hence poor adhesion to the substrate and poor layer to layer bonds. In general, a standoff distance of about the same size as the nozzle diameter is recommended in order to achieve continuous ink filament, improve layer to layer bonds, as well as adhesion to the substrate, and avoid deposition time delay[58, 59, 85, 86]. In order to accurately control the standoff distance (e.g.,  $<1\mu\text{m}$ ), a high magnification telescopic lens is usually employed which also serves a secondary purpose of visualizing ink meniscus formed between the nozzle tip and the substrate[87]. Other systems incorporate a precision height sensor for the Z-stage. Here the sensor scans the surface of the substrate prior to deposition and adjusts the nozzle tip to the set value without damaging it [58]. However, the downside of such advanced systems is that it increases the machine cost ( $\sim\$200,000$ ) and offer limited room for modification.

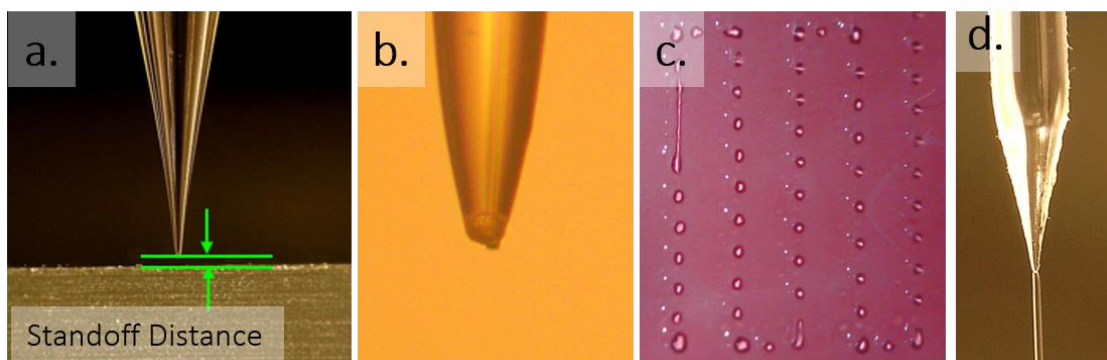


**Figure 8: Illustration of standoff distance optimization (a) Nozzle-substrate alignment to achieve optimum standoff distance, (b) Standoff distance too small leading to the broken nozzle; (c) Standoff distance too large leading to discrete droplets, (d) Proper standoff distance produces continuous ink filament.**

### 2.3.2. Effect of a Translating Substrate

To address the question, *does the substrate translating speed drive ink flow from the nozzle?* Our guiding hypothesis is that, at low flow rates, if the substrate's speed exceeds the flow speed ( $v$ ), then ink is drawn out of the nozzle by the translating substrate. As used here, low flow rate refers to creeping flows (or Stokes flow). Flows in which the Reynolds number (i.e.,  $Re = \rho v D / \mu$ ),  $Re < 10^{-1}$  are classified as Stokes flows, so that viscous forces dominate over inertial forces, which is a characteristic of very high viscosities, very low flow velocities, or flow in micro/nano length scales[88]. While low flow rates may give rise to dripping droplets and capillary effects (see section 2.2.1.), for high flow rates, inertial forces dominate, and the flow is characterized by high flow velocity which may cause unstable ink jetting and poor printing resolution[89]. Either way, the printing parameters must be carefully controlled to achieve fine prints. The possibility of ink being drawn out by a translating plate was first demonstrated by Landau and Levich [90], who developed a theoretical model for predicting the liquid film thickness formed on a plate that is vertically withdrawn from a solution reservoir at a constant speed. Subsequent works have detailed the application of this technique for controlled thin film deposition (in the case of horizontal plate motion), in a deposition technique termed “meniscus guided coating” [91, 92], as well the meniscus guided printing [77, 78] techniques. Of these techniques, the meniscus guided printing

could be likened to the  $\mu$ EP printing technique, only that it relies on low viscosity solution-based ink and at low flow rates, in which case the rapid solvent evaporation is exploited to create freestanding 3D structures.

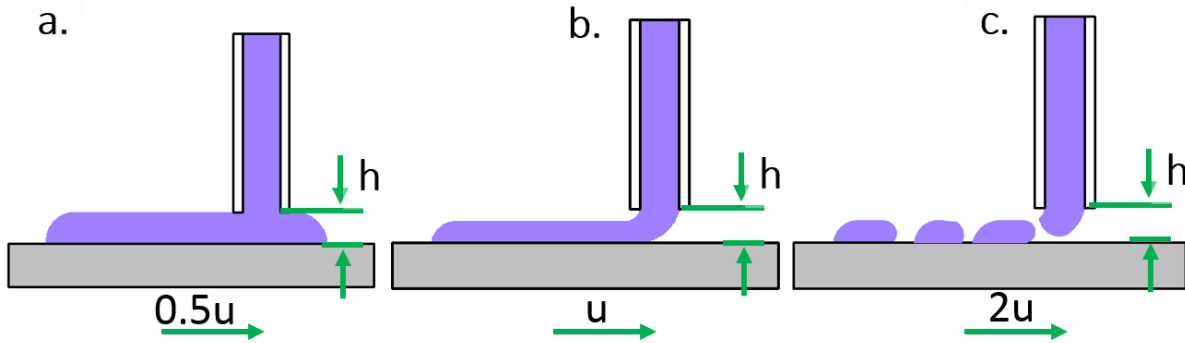


**Figure 9: Schematic illustration of the effect of printing speed at a constant flow rate and standoff distance - (a) printing speed to low resulting in smearing of the ink filament, (b) proper printing speed, (c) printing speed to high resulting in discontinuous ink filament.**

In general, similar to Eq. 12, the observed pattern is that, at a constant flow rate and standoff distance, there is critical printing speed at which the filament diameter equals the nozzle diameter, defined by Eq. 13 [19, 22].

$$u_c = \frac{Q}{Dh} \quad (13)$$

The physical meaning of this equation is that the ink flow rate ( $Q$ ) determines the amount of material available for deposition within a given space and time. If the printing speed is less than this value, the ink filament may be compressed resulting in forced flow (Figure 9a). On the other hand, while faster printing speed is usually preferred to reduce build time, if it is greater than the critical value, a stretching effect will be induced in the ink (Figure 9b). A further increase in speed may result in unstable and discontinuous prints (Figure 9c). Filament breakup process has been studied extensively and could be likened the uniaxial pulling of liquid sandwiched between two pistons. As the ink is being stretched, it undergoes a progressive necking (thinning) and subsequent breakup. As the ink is being stretched, it undergoes a progressive necking (thinning) and subsequent breakup, but there is no clear-cut mark as to when discontinuity or breakup begins but is found to be a function of Webber number, Reynolds number and strain rate [19, 22, 93-95].

In an attempt to model the ink deposition process, Vozzi et al. [53] only considered the applied pressure as the primary driving force, in which case the model failed to accurately predict feature resolution at low flow rates, where other factors like substrate velocity and surface forces may have been influential. One possible explanation for the observed results is that at low flow rates, the substrate may play a significant role in pulling ink out of the deposition nozzle. To this end, we adopt an experimental technique to validate our guiding hypothesis using PDMS ink. We accomplished this by measuring flow rates through a  $10\mu\text{m}$  nozzle at different speeds of the substrate. The mass flow rate was measured by dividing the mass of printed feature by the time taken to print them. The measuring balance has a readability of  $10\mu\text{g}$ . The printing process was

carried out using a custom-made 3-axis Microextrusion printer, which has a 50nm resolution for the three axes. The experimental condition is presented in Table 3, while printing process and the plot of flow rate as a function of printing speed are shown in Figure 10.

**Table 3: Experimental conditions for the effects of translating substrate experiment**

Ink	Viscosity (cP)	Standoff distance	Applied pressure	Substrate speed
Sylgard 184 (part A)	5100	~10 $\mu$ m	1psi	0-0.075mm/s

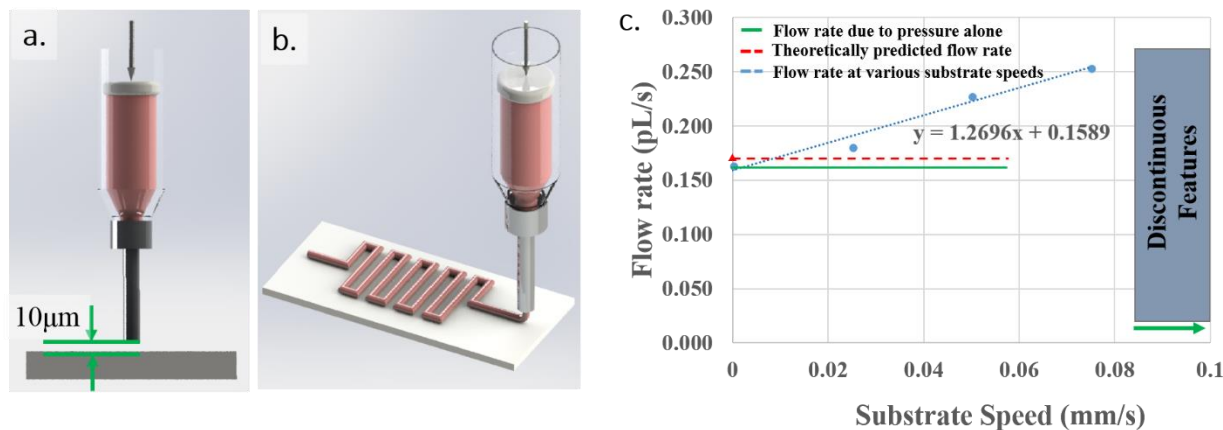


**Figure 10: Schematic illustration of the microextrusion printing process (a) Standoff distance measurement, (b) Patterned hairpin structure on a glass substrate, and (c) Measured flow rate as a function of substrate speed. Each data point is an average of four different experimental results**

The most important point revealed Figure 10c is the flow rate – substrate speed dependence. This validates our hypothesis that if the substrate’s speed exceeds the ink flow rate, then ink is drawn out of the nozzle by the translating substrate. The dotted horizontal line represents experimentally determined flow rate at zero substrate speed. Clearly, the flow rate increased from 0.164 to 0.254pL/s (~55.1%) as the substrate speed was increased from 0 to 75 $\mu$ m/s, which agrees with our hypothesis. The experimentally determined flow rate due to pressure alone (0.164pL/s) is also in close agreement with the theoretically predicted value based on Eq. 4 (0.166pL/s). The difference between the two values is 0.019pL/s (~1.2%), indicating the experimentally determined flow rates are reliable. A line of best fit applied to the result reveals the flow rate changes linearly with substrate speed. This result holds important implication for  $\mu$ EP, that is, if a very viscous material needs to be printed but the pressure is limited, the deposition process can be driven by a combination of the extrusion pressure and substrate speed.

#### 2.4. Phase 4 (P<sub>4</sub>): Time-Dependent Wetting and Drying

The interaction between the ink, the ambient air around it, and the surface properties of the substrate play a critical role in determining the final print quality. The dynamics of this phenomenon at the microscale is markedly different from that at the macroscale due to the dominance of the surface tension force arising from the higher surface area to volume ratio. Hence, print resolution, geometry, adhesion to the substrate, and drying rate can be directly inferred from the rheological ink properties, surface properties of the substrate, as well as the prevailing ambient

condition. The contact angle is the primary quantitative parameter used to predict or quantify the effect of this interaction. To this end, our discussion will be divided into two categories: (2.4.1.) surface energy interaction, and (2.4.2.) contact angle hysteresis.

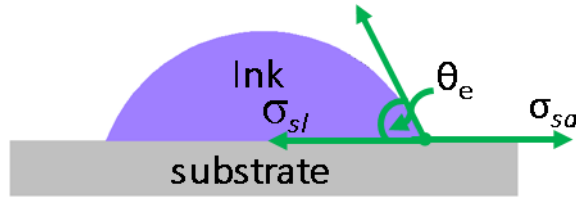


**Figure 11: Schematic illustration of ink-substrate interaction with an equilibrium contact angle**

As shown in Figure 11 contact angle is defined as the angle created by the intersection of the link-substrate interface, and the link-air interface. Here, we distinguish between the two types of contact angles – static and dynamic. The static contact angle describes the angle formed when the three-phase contact line is not moving, while the dynamic contact angle occurs when the three-phase contact line is moving.

#### 2.4.1. Surface Energy Effect

The degree at which ink wets the substrate is governed by the ink-substrate interaction and is usually measured by the equilibrium (static) contact angle ( $\theta_e$ ). According to Young's equation (for a smooth surface), the wetting characteristics relating the surface energy to the equilibrium contact angle where the three phases are in mechanical equilibrium with each other is given by [96, 97]:

$$\sigma_{sa} = \sigma_{sl} + \sigma_{la} \cos \theta_e \quad (14)$$

Where  $\sigma_{sa}$ ,  $\sigma_{sl}$ , and  $\sigma_{la}$  represents the interfacial energy between substrate and air, the substrate and liquid, and liquid and air respectively. As a rule of thumb, if the ink is too fluidic, there will be extensive spreading, which is aggravated if the surface energy of the substrate is far greater than that of ink. Conversely, if the ink is on the upper end of the viscosity spectrum, it beads up, which may cause a discontinuity in the ink filaments and poor adhesion to the substrate. Therefore, a limited degree of ink fluidity is often desirable to ensure filament continuity and adhesion [19, 60, 98].

#### 2.4.2. Contact Angle Hysteresis

Unlike Young's equation which ascribes a unique contact, on real surfaces, there exist many metastable states giving rise to dynamic contact angle. This variation results from surface imperfections (e.g., surface roughness or inhomogeneity). Consequently, a static angle does not provide enough description of the wetting behavior [99]. For example, after deposition on the substrate, a Non-Newtonian ink may expand or contract to give rise to a spectrum of shapes and contact angle. The contact angle formed because the expansion of ink filament is known as the advancing contact angle ( $\theta_a$ ). In contrast, the contact angle resulting from contraction of ink filament is referred to as receding contact angle ( $\theta_r$ ). So, in practice, the final contact angle has a value between the advancing and receding contact angle (with  $\theta_a > \theta_r$ , and contact angle hysteresis

is a term used to describe this phenomenon, which is the difference between the advancing and receding contact angle (Figure 12):

$$H = \theta_a - \theta_r \quad (15)$$

During this process, the imperfection of the substrate surface act as barriers to pin the motion of the contact line fronts (either in the advancing or receding direction) and it is this pinning effect which gives rise to increase or decrease in the observed contact angle.

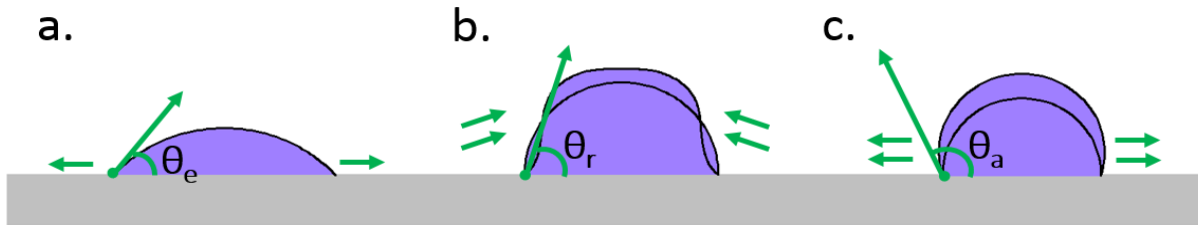


**Figure 12: Illustration of contact angle hysteresis – (a) Equilibrium contact angle, (b) Receding contact angle, (c) Advancing contact angle**

Taking surface energy effects and contact angle hysteresis together, we discuss their implications for microextrusion printing. A small contact angle (i.e.,  $\theta \rightarrow 0^\circ$ ) is indicative of a strong ink-substrate interaction (see Eq. 14), with maximum possible spreading until an equilibrium configuration which minimizes the surface energy is attained (Figure 12a). This type of behavior is typical of Newtonian inks which have low viscosity, low surface energy relative to the substrate, and the final shape is determined by the difference in surface energy between ink and substrate. For non-Newtonian inks (shear thinning inks) which typically have high viscosity, the strong cohesive interparticle forces which increase with filament volume inhibits ink spreading. However, with microscale printing involving small ink volume, the surface tension force tends to dominate over the cohesive force. More so, because ink rheology varies with shear rate during extrusion, with the maximum occurring at the nozzle tip and decreasing to zero after contacting the substrate, the deposited filament is prone to spread, and contract before settling [19, 62]. For instance, with appropriate ink rheology, the filament may contract after deposition to yield a nearly rectangular cross-sectional area with a flattened top (i.e.,  $0^\circ < \theta_r \leq 90^\circ$ , Figure 12b). On the other hand, if the ink is too fluidic, and the standoff distance and printing speed are not well matched, this can cause swelling (or expansion) of the ink filament resulting in a rounded structure (i.e.,  $90^\circ < \theta_a < 180^\circ$ , Figure 12c) [60, 100, 101].

Beyond these, the literature is widespread with examples indicating the crucial influence of substrate on print resolution. In particular, the influence of low and high energy surfaces, as well as porous and non-porous substrates have been studied, and have been found to either aid or limit spreading [98, 102, 103]. For example, Boley et al. studied the contact angle of printed gallium-indium alloy inks on glass and PDMS substrates [103]. As expected, the glass substrate exhibited higher wetting (i.e., a lower contact angle) due to its higher surface energy compared to PDMS. King et al. demonstrated the case of a porous (FR4) and non-porous (alumina), in which silver paste was printed on both substrates. Their results indicated a shrinkage, and longer spreading time on alumina substrate compared to FR4 substrate (Figure 13). This observation is attributed to the additional solvent lost provided by the more porous FR4 surface [61]. In another study, Perez et al. employed heated substrates to increase solvent drying [104]. However, heating the substrates

should be done cautiously because a fast-drying rate can result in cracking, warping and delamination[60] of the printed structures.

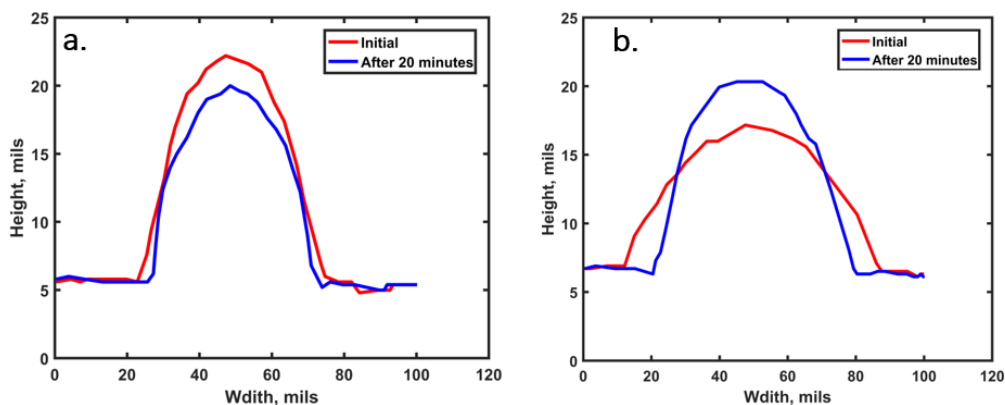


**Figure 13: Profile of silver paste printed on (a) FR4 substrate, and (b) alumina substrate as a function of time**

As evident from the foregoing discussions, there are three primary methods of controlling the shape and resolution of the prints: (1) Treating the substrate with hydrophobic materials to create a low energy surface will limit excessive spreading of low-viscous inks, (2) As reported by Liang et al. [98] using highly viscous inks in place of surface modification of the substrate will generally yield better output than substrate treatment, (3) Surface properties of the substrate (e.g., porosity, irregularity of the surface) is the main driver for hysteresis effect and would determine final print geometry. In addition, faster drying may be achieved by using a porous substrate to provide additional channels to drive out the solvent.

### III. APPLICATION

To demonstrate the usefulness of the presented framework in section II, we will provide a case study of achieving  $\mu$ EP of high-resolution features using PDMS ink based on knowledge gained from this framework. In section 3.1 we discuss the rationale for choosing PDMS as the material for this demonstration, and present the results and discussions in section 3.2.

#### 3.1 Materials and Methods

Occasioned by its biocompatibility, optical transparency, and tunable mechanical properties, there has been a growing demand for high-resolution, and low-cost patterning polydimethylsiloxane (PDMS) elastomer-based structures. Such structures have widespread applications including biosensors [105], general cell study (e.g., DNA and proteins) self-assembled monolayers (SAMs)[106, 107], and wearable electronics[108]. While Soft-lithography has been well-developed for creating patterns from this “mechanically soft materials”, the need of making masks, usage of cleanroom equipment, and long process cycles make it costly. Extrusion-based printing technique provides an alternative solution for making PDMS structures. However, its adoption has been hindered due to (1) the poor resolution of commercial 3D printers, and (2) the lack of ideal PDMS printing properties. To circumvent this second problem, several variants of this printing technique have been tested in order to improve print resolution and fidelity. For

example, one approach prints PDMS within a support bath; thus, providing the needed mechanical support to hold the structure in place until it is cured and is subsequently removed. However, a drawback of this technique is that the interfacial interactions between the support bath materials and the PDMS could influence the morphology of the printed structures, and several difficulties were experienced during removal from the support material [109]. To offer a low-cost PDMS printing platform, Structur3D Printing company came up with the Discov3ry Paste Extruder, as a universal add-on for commercial FDM printers, but this system is better suited for printing mesoscale structures ( $\sim 250\mu\text{m}$ )[110]. Still, several applications require PDMS patterns in the micrometer length scale, and to our knowledge, this is yet to be demonstrated by any 3D printing approach.

Herein, we demonstrate the viability of  $\mu\text{EP}$  to pattern microscale PDMS features with two objectives. First, to overcome the limitations arising from the non-ideal ink property, we developed an empirical model to predict viscosity-time relationship, which is used to adjust the printing process parameters to overcome capillary rise effect and surface wetting. Second, to improve printing resolution, alleviate the fabrication challenges, and lower the cost of patterning high-resolution PDMS, we employed a custom-made  $\mu\text{EP}$  developed in our group. We demonstrate this strategy using Sylgard 184 (Dow Corning), which is the commonly used PDMS for soft-lithography processes, and for making biomedical templates [111]. The PDMS ink was prepared by mixing a 10:1 ratio of part A (base) and B (curing agent) respectively; and subsequently degassed to eliminate air bubbles. The air-free mixture was then utilized for both the rheological characterization and microextrusion printing. In the sections following, we will discuss the stepwise approach to achieving a target feature resolution of  $\sim 10\mu\text{m}$ . Throughout this section, a  $5\mu\text{m}$  nozzle size will be applied utilized.

## **3. 2. Results and Discussions**

In this section, we present the results of the printing process guided by the four phases established in the presented framework. For this demonstrative application, simple planar, and 2D grid structures are printed.

### ***3.2.1. Phase 1: Ink Flow Behavior***

Sylgard 184 is a two-part liquid that exhibits a modest viscosity at room temperature. However, once mixed it undergoes gelation over time (under ambient conditions), and viscosity increases by several orders of magnitude, which dictates printability. In order to effectively use this material for  $\mu\text{EP}$ , we needed a means of predicting the rate at which viscosity changes over time. To this end, we sought to develop a model to predict the viscosity-time relationship. We measured the rheological properties of this ink using a rheometer (Brookfield DV3T LV). First, to reveal any shear rate dependence, ink viscosity was characterized at a controlled shear rate mode ranging from  $0.034$  to  $2.04\text{s}^{-1}$ . To reduce variability in the measurement results a single point averaged value for each set of condition was obtained over a 2-minute period. Second, to capture any possible time-dependent property, six different measurements, at each shear rate was performed at 30 minutes intervals. All measurements were done at  $24.2^\circ\text{C}$ . From this data, ink flow behavior is identified and presented in Figure 14.

As shown in Figure 14 **Figure 14(a)**, the ink displays a slight increase in apparent viscosity with increasing shear rate. For instance, as the shear rate increased from 0.17 to 1.53s<sup>-1</sup>, the viscosity increased by

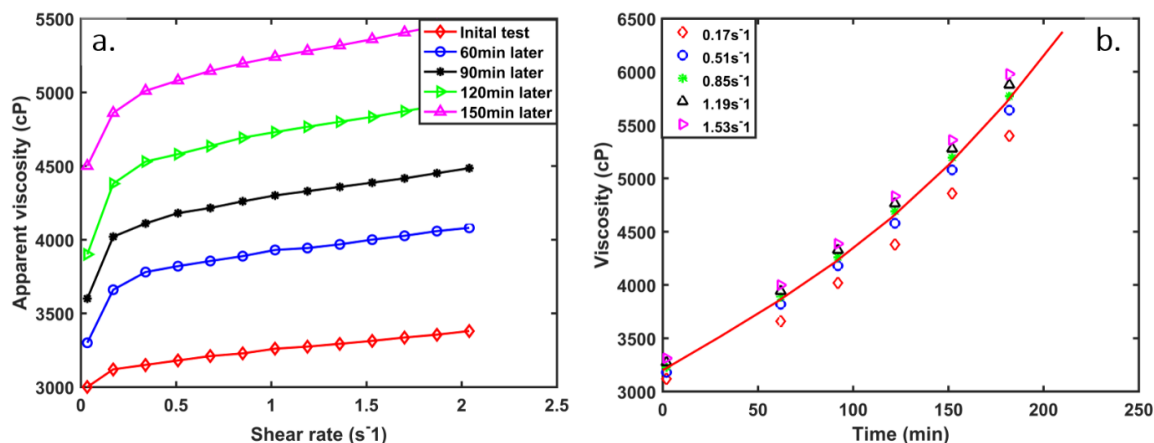


**Figure 14: Apparent viscosity of Sylgard 184 as (a) a function of the shear rate for 30 minutes time steps (b) as a function of curing time for different shear rates, at Temp. of 24.2°C. The points refer to experimental data and the solid line represents the model.**

6.19%, as opposed to 800% increase in shear rate (**Error! Reference source not found.**). Interestingly, within the range of tested shear rate, the viscosity was observed to be almost independent of shear rate, implying a Newtonian flow behaviour **Figure 14Figure 14(a)**, which agrees with the finding by Schneider et al. [112]. Next, given the possibility of the dependence of viscosity on time, we then sought to quantify this relationship, and **Figure 14Figure 14(b)**, confirms a clear rheopectic behavior (i.e., a time-dependent shear thickening). For instance, at a shear rate of 0.170s<sup>-1</sup>, the viscosity increased by ~73% over 180 min., which is far greater than the influence due to shear rate (**Error! Reference source not found.**).

This flow behavior has several implications for μEP: (1) the viscosity increases continuously throughout the printing process, (2) a constant value of viscosity cannot be used to predict flow rate, (and hence feature resolution), (3) for long printing times, the deposition pressure needs to be constantly increased in order to achieve a constant flow rate. Recognizing this significant viscosity-time dependence, and the prospect of achieving stable structures, we developed a model (based on **Figure 14b**) for predicting ink viscosity as a function of time. The 4<sup>th</sup>-degree interpolation polynomial below describes the viscosity-time relationship.

$$\mu(t) = 3202 + 10.5t - 5.43 \times 10^{-3}t^2 + 1.73 \times 10^{-4}t^3 - 1.79 \times 10^{-7}t^4 \quad (16)$$

**Table 4: The Estimated increasing rate of viscosity as a function of shear rate**

Shear	Viscosity (cP)	% increase in viscosity
0.17	3120	-
0.51	3180	1.9
1.19	3274	4.94
1.53	3313	6.19

This model which is based on averaged experimental data was found to accurately approximate ink viscosity, for the range of shear rates studied here. For very short printing times, the terms with higher powers of  $t$  tend to zero, and viscosity may be considered relatively constant. Under this condition using Eq. 3, (with  $t=5$  min.,  $D=5\mu\text{m}$ ,  $L=3\text{mm}$ ,  $\Delta P=100\text{psi}$ ) the flow rate was calculated to be  $\approx 17.3\text{pl/s}$ .

**Table 5: The Estimated increasing rate of viscosity as a function of time**

Time (min)	Viscosity (cP)	% increase in viscosity
2	3120	-
90	4020	28.84
120	4380	40.38
180	5400	73.08

### 3.2.2. Phase 2: Capillary Rise and Evaporative Effect

One of the primary objectives for viscosity pre-calibration carried out in section 3.2.1 was to increase the PDMS viscosity, and hence limit the degree of the capillary effect. To achieve this, we allowed ample time (7 hours) for the ink to cure, during which viscosity increased from 3202 to 13679cP ( $\sim 4.3$ -fold increase). Under this condition, the ink rheology change from liquid to gel-like behavior. The capillary number ( $Ca$ ) was computed to be  $9.1 \times 10^{-6}$  (using  $\sigma = 19.8$  mN/m[113],  $v = 1.34 \times 10^{-7}$  mm/s,  $\mu = 13,679$  cP) which is far less than the threshold value predicted by our theory. Therefore, as the theory predicts, with ink of low viscosity and low surface energy if the nozzle has a higher surface energy than the ink, and  $Ca < 10^{-1}$  then the ink may wet the nozzle surface, giving rise to high capillary effect.

Evidently, the large increase in viscosity reduced excessive capillary effect but did not eliminate it as can be inferred from the low capillary number. To overcome any possible capillary effect, it became clear that consistent and reproducible features could obtain by carefully bringing the nozzle tip close to the substrate so that it directly contacts the substrate once it exits the nozzle tip and is drawn along the substrate. At the printing condition (i.e.,  $T = 24^\circ\text{C}$ ) it took about 10 hours for the ink to not be extrudable while the flow timescale  $t_{\text{flow}}$  is  $\sim 18.6$  s. This means a small flow timescale relative to curing timescale, therefore, we do not expect rapid curing to be to become a problem. However, in the primary experiment it was realized that if a heated substrate was employed, ink curing time reduced drastically leading to clogging of the nozzle tip.

### 3.2.3. Phase 3: Standoff Distance and Printing Speed

Guided by our framework, we started out with the same standoff distance as the nozzle diameter (i.e.,  $h = 5\mu\text{m}$ ) which was observed to give consistent extrusion. The nozzle-substrate alignment process was carried with the aid of a microscope. With an estimated flow rate of  $2.63\text{fL/s}$ , using Eq. 13 (i.e.,  $u_c = Q/D \cdot h$ ), the critical printing speed was calculated to be  $\sim 0.126\mu\text{ms}^{-1}$ . Using this value and  $10\mu\text{m}$  standoff distance, the printer was then operated in an automatic mode to sequentially execute the scripted g-code, while varying the printing speed until the minimum line width was obtained.

### 3.2.4. Phase 4: Substrate Choice

Based on the interaction between nozzle and substrate, it became obvious that a glass substrate has a high surface energy relative to the ink (i.e.,  $\sigma_{e(\text{glass})} = 310\text{mN/m}$ ,  $\sigma_{e(\text{glycerol})} = 70.9\text{mN/m}$ ) and would therefore induce a large degree of spreading. For this reason, a PET with a lower surface energy substrate ( $\sigma_{e(\text{PET})} = 41\text{mN/m}$ ) was selected for the substrate. After the printing, the sample cured at room temperature for 24 hours, and the representative results are presented in Figure 15.

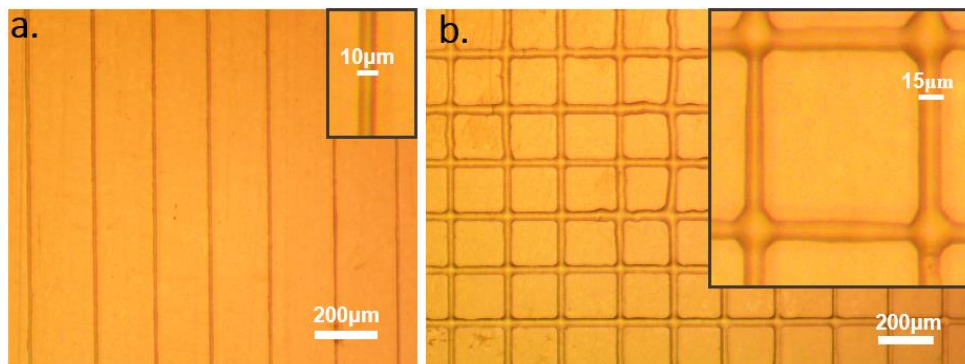


**Figure 15: (a) Photomicrographs of micro-patterns patterns on PET substrate (a) Planar array of patterned PDMS with 200µm center-to-center spacing, (b) Square grids of patterned PDMS with a 200µm center-to-center spacing. Printing conditions: 10µm nozzle at the 1psi and 0.1mm/s.**

We patterned planar arrays of the PDMS filaments with a center-to-center spacing of 200µm (Figure 15a), 2D square grids (Figure 15b). The printed patterns have widths ~10µm. These results show the ability of the µEP technique to pattern high-resolution features. This printing technique may find a niche in tissue engineering, for fabricating porous biological scaffold materials and elastomeric stamps for patterning various chemicals.

## IV. CONCLUSIONS AND FUTURE OUTLOOK

This review was motivated by the lack of comprehensive understanding of the dynamic intricacies that underscore successful microextrusion printing and was therefore aimed at providing users with the requisite knowledge base needed for adapting µEP for microfabrication. Ultimately, this understanding and control of the various materials and process parameters dictate the resolution and quality of the printed features. This printing techniques drastically simplifies the fabrication of arbitrary structures, and a wide range of choices in materials and substrates, when compared to the classical photolithography techniques.

Overall, we set out to investigate four important question: (1) *what are the ink properties that determine printability, and shape retention characteristics?* The ideal ink for µEP must satisfy several criteria including ability to flow easily through fine needles when subjected to a shear force, good shape retaining ability after extrusion and self-supportability, which are readily satisfied by shear thinning inks with high viscoelastic properties. (2) *what are the dominant driving forces that govern ink extrusion at the microscale?* Results from the literature showed that, generally, ink viscosity and nozzle geometric features play significant roles in driving flow.

However, at the length scale of our consideration, the roles of surface forces, and translating speed of the substrate increases, while the effect of gravity is negligible, and therefore demands careful control in order to achieve desired flow rates. (3) *What are the major factors that determine the final resolution of printed tracks?* We identified the impacts of three significant process parameters (e.g., standoff distance, substrate speed and substrate surface property) on feature resolution. The finding is that high standoff distance or high substrate speed can result in discontinuous features, while a small standoff distance or low printing speed can result in forced spreading and over deposition respectively. Eq. 12 and 13 are proposed to guide the selection of the optimum standoff distance and substrate speed. The substrate surface property is characterized mainly by the advancing and receding contact angles, which play a significant role in determining the final printing resolution. (4) *How do we modulate these factors to meet the requirements of target applications?* Armed with the above knowledge, we provided a stepwise approach on how the various factors can be modulated to achieve high resolution features with conventional PDMS materials. We patterned microperiodic structures PDMS structures with resolution down to  $\sim 10\mu\text{m}$ , which proved challenging for previous works.

Despite the progress that has been made, there are many opportunities for improvements for  $\mu\text{EP}$ , including better understanding and control of tool pathways, the need for more precise ink flow prediction to fabricate more sophisticated geometries. The drive for finer feature sizes sacrifices the printing speeds and improving printing speed could facilitate widespread adoption of this patterning technique. Further development and exploration of novel materials with requisite properties are at the center of furthering this printing technology.

## V. Acknowledgments

We are thankful to our colleagues at the AM<sup>3</sup> Lab for providing support and enabling environment for this work. We gratefully acknowledge the financial support from the University of Arkansas, through the startup fund provided by the Vice Provost Office for Research and Economic Development. Any opinions, findings, and conclusions or recommendations expressed in this publication are those of the authors and do not necessarily reflect the views of the University of Arkansas.

## VI. References

- [1] Hsu, T., 2002, "Miniaturization—A paradigm shift in advanced manufacturing and education," International conference on Advanced Manufacturing Technologies and Education in the 21st Century.
- [2] Ikuta, K., Hirowatari, K., and Ogata, T., 1994, "Three-dimensional micro integrated fluid systems (MIFS) fabricated by stereo lithography," Micro Electro Mechanical Systems, 1994, MEMS'94, Proceedings, IEEE Workshop on, Anonymous IEEE, pp. 1-6.
- [3] Sun, K., Wei, T., Ahn, B. Y., 2013, "3D Printing of Interdigitated Li-ion Microbattery Architectures," *Advanced Materials*, 25(33) pp. 4539-4543.
- [4] Wehner, M., Truby, R., Fitzgerald, D., 2016, "An Integrated Design and Fabrication Strategy for Entirely Soft, Autonomous Robots," *Nature*, 536(7617) pp. 451-451.
- [5] Hardin, J. O., Ober, T. J., Valentine, A. D., 2015, "Microfluidic Printheads for Multimaterial 3D Printing of Viscoelastic Inks," *Advanced Materials*, 27(21) pp. 3279-3284.
- [6] Chou, H. P., Spence, C., Scherer, A., 1999, "A Microfabricated Device for Sizing and Sorting DNA Molecules," *Proceedings of the National Academy of Sciences of the United States of America*, 96(1) pp. 11-13.
- [7] Dario, P., Carrozza, M. C., Benvenuto, A., 2000, "Micro-Systems in Biomedical Applications," *Journal of Micromechanics and Microengineering*, 10(2) pp. 235.
- [8] Hansen, C. J., Wu, W., Toohey, K. S., 2009, "Self-Healing Materials with Interpenetrating Microvascular Networks," *Advanced Materials*, 21(41) pp. 4143-4147.

- [9] Chabynyc, M. L., Chiu, D. T., McDonald, J. C., 2001, "An Integrated Fluorescence Detection System in Poly (Dimethylsiloxane) for Microfluidic Applications," *Analytical Chemistry*, 73(18) pp. 4491-4498.
- [10] Weigl, B. H., and Yager, P., 1999, "Microfluidic Diffusion-Based Separation and Detection," *Science*, 283(5400) pp. 346-347.
- [11] Anderson, J. R., Chiu, D. T., Jackman, R. J., 2000, "Fabrication of Topologically Complex Three-Dimensional Microfluidic Systems in PDMS by Rapid Prototyping," *Analytical Chemistry*, 72(14) pp. 3158-3164.
- [12] Ahn, B. Y., Duoss, E. B., Motala, M. J., 2009, "Omnidirectional Printing of Flexible, Stretchable, and Spanning Silver Microelectrodes," *Science (New York, N.Y.)*, 323(5921) pp. 1590-1593.
- [13] Kim, J. T., Seol, S. K., Pyo, J., 2011, "Three-Dimensional Writing of Conducting Polymer Nanowire Arrays by Meniscus-Guided Polymerization," *Advanced Materials*, 23(17) pp. 1968-1970.
- [14] Sirringhaus, H., Kawase, T., Friend, R. H., 2000, "High-Resolution Inkjet Printing of all-Polymer Transistor Circuits," *Science (New York, N.Y.)*, 290(5499) pp. 2123-2126.
- [15] Gibson, I., Rosen, D.W., and Stucker, B., 2010, "Additive manufacturing technologies," Springer, .
- [16] Sirringhaus, H., Kawase, T., Friend, R. H., 2000, "High-Resolution Inkjet Printing of all-Polymer Transistor Circuits," *Science (New York, N.Y.)*, 290(5499) pp. 2123-2126.
- [17] Barton, K., Mishra, S., Shorter, K. A., 2010, "A Desktop Electrohydrodynamic Jet Printing System," *Mechatronics*, 20(5) pp. 611-616.
- [18] Kadara, R. O., Jenkinson, N., Li, B., 2008, "Manufacturing Electrochemical Platforms: Direct-Write Dispensing Versus Screen Printing," *Electrochemistry Communications*, 10(10) pp. 1517-1519.
- [19] Wang, J., and Shaw, L. L., 2005, "Rheological and Extrusion Behavior of Dental Porcelain Slurries for Rapid Prototyping Applications," *Materials Science and Engineering: A*, 397(1) pp. 314-321.
- [20] Lewis, J. A., and Gratson, G. M., 2004, "Direct Writing in Three Dimensions," *Materials Today*, 7(7) pp. 32-39.
- [21] Therriault, D., Shepherd, R. F., White, S. R., 2005, "Fugitive Inks for Direct-Write Assembly of Three-Dimensional Microvascular Networks," *Advanced Materials*, 17(4) pp. 395-399.
- [22] Khalil, S., and Sun, W., 2007, "Biopolymer Deposition for Freeform Fabrication of Hydrogel Tissue Constructs," *Materials Science and Engineering: C*, 27(3) pp. 469-478.
- [23] Vozzi, G., Flaim, C., Ahluwalia, A., 2003, "Fabrication of PLGA Scaffolds using Soft Lithography and Microsyringe Deposition," *Biomaterials*, 24(14) pp. 2533-2540.
- [24] Vozzi, G., Previti, A., De Rossi, D., 2002, "Microsyringe-Based Deposition of Two-Dimensional and Three-Dimensional Polymer Scaffolds with a Well-Defined Geometry for Application to Tissue Engineering," *Tissue Engineering*, 8(6) pp. 1089-1098.
- [25] Schaffner, M., Ruhs, P. A., Coulter, F., 2017, "3D Printing of Bacteria into Functional Complex Materials," *Science Advances*, 3(12).
- [26] Schuurman, W., Levett, P., Pot, M., 2013, "Gelatin-Methacrylamide Hydrogels as Potential Biomaterials for Fabrication of Tissue-Engineered Cartilage Constructs," *MACROMOLECULAR BIOSCIENCE*, 13(5) pp. 551-561.
- [27] Kang, H., Lee, S., Ko, I., 2016, "A 3D Bioprinting System to Produce Human-Scale Tissue Constructs with Structural Integrity," *Nature Biotechnology*, 34(3) pp. 312-312.
- [28] Jin, Y., Plott, J., and Shih, A., 2015, "Extrusion-based additive manufacturing of the moisture-cured silicone elastomer," *Proc. Solid Free. Fabr. Symp*, Anonymous pp. 308-318.
- [29] Bhattacharjee, T., Zehnder, S. M., Rowe, K. G., 2015, "Writing in the Granular Gel Medium," *Science Advances*, 1(8) pp. e1500655.
- [30] Hinton, T. J., Hudson, A., Pusch, K., 2016, "3D Printing PDMS Elastomer in a Hydrophilic Support Bath Via Freeform Reversible Embedding," *Acs Biomaterials Science & Engineering*, 2(10) pp. 1781-1786.
- [31] Dermanaki-Farahani, R., Lebel, L. L., and Therriault, D., 2014, "Manufacturing of Three-Dimensionally Microstructured Nanocomposites through Microfluidic Infiltration," *Journal of Visualized Experiments: JoVE*, (85). doi(85) pp. 10.3791/51512.
- [32] Sun, K., Wei, T., Ahn, B. Y., 2013, "3D Printing of Interdigitated Li-Ion Microbattery Architectures," *Advanced Materials*, 25(33) pp. 4539-4543.
- [33] Malone, E., Rasa, K., Cohen, D., 2004, "Freeform Fabrication of Zinc-Air Batteries and Electromechanical Assemblies," *Rapid Prototyping Journal*, 10(1) pp. 58-69.
- [34] Kuhn, M., Napporn, T., Meunier, M., 2008, "Direct-Write Microfabrication of Single-Chamber Micro Solid Oxide Fuel Cells," *Journal of Micromechanics and Microengineering*, 18(1) pp. 015005.

- [35] Becerril, H. A., Roberts, M. E., Liu, Z., 2008, "High-Performance Organic Thin-Film Transistors through Solution-Sheared Deposition of Small-Molecule Organic Semiconductors," *Advanced Materials*, 20(13) pp. 2588-2594.
- [36] Dimos, D., King, B., and Yang, P., 1999, "Direct-write fabrication of integrated, multilayer passive components," *Advanced Packaging Materials: Processes, Properties and Interfaces*, 1999. Proceedings. International Symposium on, Anonymous IEEE, pp. 186-190.
- [37] Ahn, B. Y., Lorang, D. J., Duoss, E. B., 2010, "Direct-Write Assembly of Microperiodic Planar and Spanning ITO Microelectrodes," *Chemical Communications*, 46(38) pp. 7118-7120.
- [38] Ahn, B. Y., Duoss, E. B., Motala, M. J., 2009, "Omnidirectional Printing of Flexible, Stretchable, and Spanning Silver Microelectrodes," *Science (New York, N.Y.)*, 323(5921) pp. 1590-1593.
- [39] Massa, S., Sakr, M. A., Seo, J., 2017, "Bioprinted 3D Vascularized Tissue Model for Drug Toxicity Analysis," *Biomicrofluidics*, 11(4) pp. 044109.
- [40] Therriault, D., White, S. R., and Lewis, J. A., 2003, "Chaotic Mixing in Three-Dimensional Microvascular Networks Fabricated by Direct-Write Assembly," *Nature Materials*, 2(4) pp. 265-271.
- [41] Wu, W., 2010, "Direct ink writing of microvascular networks," University of Illinois at Urbana-Champaign.
- [42] Therriault, D., 2003, "Directed assembly of three-dimensional microvascular networks".
- [43] Risner, J., 2008, "Investigation of dielectric elastomer actuation for printable mechatronics," University of California, Berkeley.
- [44] Muth, J. T., Vogt, D. M., Truby, R. L., 2014, "Embedded 3D Printing of Strain Sensors within Highly Stretchable Elastomers," *Advanced Materials*, 26(36) pp. 6307-6312.
- [45] Lewis, J. A., 2006, "Direct Ink Writing of 3D Functional Materials," *Advanced Functional Materials*, 16(17) pp. 2193-2204.
- [46] Datar, A., 2012, "Micro-extrusion process parameter modeling," Rochester Institute of Technology.
- [47] Gleadall, A., Ashcroft, I., and Segal, J., 2018, "VOLCO: A Predictive Model for 3D Printed Microarchitecture," *Additive Manufacturing*, 21 pp. 605-618.
- [48] Mason, M. S., Huang, T., Landers, R. G., 2006, "Freeform extrusion of high solids loading ceramic slurries, Part I: Extrusion process modeling," 17th Solid Freeform Fabrication Symposium, SFF 2006, August 14, 2006 - August 16, Anonymous University of Texas at Austin (freeform), Austin, TX, United states, pp. 316-328.
- [49] Li, Q., and Lewis, J. A., 2003, "Nanoparticle Inks for Directed Assembly of Three-Dimensional Periodic Structures," *Advanced Materials*, 15(19) pp. 1639-1643.
- [50] Smay, J. E., Cesarano, J., and Lewis, J. A., 2002, "Colloidal Inks for Directed Assembly of 3-D Periodic Structures," *Langmuir*, 18(14) pp. 5429-5437.
- [51] Chang, R., Nam, J., and Sun, W., 2008, "Effects of Dispensing Pressure and Nozzle Diameter on Cell Survival from Solid Freeform fabrication-based Direct Cell Writing," *Tissue Engineering Part A*, 14(1) pp. 41-48.
- [52] Cao, Y., Zhou, L., Wang, X., 2009, "MicroPen Direct-Write Deposition of Polyimide," *Microelectronic Engineering*, 86(10) pp. 1989-1993.
- [53] Vozzi, G., Previti, A., De Rossi, D., 2002, "Microsyringe-Based Deposition of Two-Dimensional and Three-Dimensional Polymer Scaffolds with a Well-Defined Geometry for Application to Tissue Engineering," *Tissue Engineering*, 8(6) pp. 1089-1098.
- [54] Crockett, R. S., and Calvert, P. D., 1996, "The Liquid-to-Solid Transition in Stereodeposition Techniques," *Solid Freeform Fabrication Symposium*, Anonymous pp. 257-264.
- [55] Piqué, A., and Chrisey, D.B., 2001, "Direct-write technologies for rapid prototyping applications: sensors, electronics, and integrated power sources," Academic press.
- [56] Anonymous 2018, "Surface Tension Values of some Common Test Liquids for Surface Energy Analysis Available: <http://www.Surface-Tension.De/>," .
- [57] Nordson EFD, 2017, "Important Safety Information," .
- [58] Li, B., Clark, P. A., and Church, K., 2007, "Robust direct-write dispensing tool and solutions for micro/meso-scale manufacturing and packaging," *ASME 2007 International Manufacturing Science and Engineering Conference*, Anonymous American Society of Mechanical Engineers, pp. 715-721.
- [59] Cao, Y., Zhou, L., Wang, X., 2009, "MicroPen Direct-Write Deposition of Polyimide," *Microelectronic Engineering*, 86(10) pp. 1989-1993.
- [60] Cesarano, J., III, Segalman, R., and Calvert, P., 1998, "Robocasting Provides Moldless Fabrication from Slurry Deposition," *Ceramic Industry*, 148(4) pp. 94-94.

- [61] King, B. H., Morissette, S., Denham, H., 1998, "Influence of rheology on deposition behavior of ceramic pastes in direct fabrication systems," *Solid Freeform Fabrication Symposium*, Anonymous pp. 391-398.
- [62] Morissette, S. L., Lewis, J. A., Cesarano, J., 2000, "Solid Freeform Fabrication of Aqueous alumina-poly (Vinyl Alcohol) Gelcasting Suspensions," *Journal of the American Ceramic Society*, 83(10) pp. 2409-2416.
- [63] Vickroy, B., Lorenz, K., and Kelly, W., 2007, "Modeling Shear Damage to Suspended CHO Cells during Cross-Flow Filtration," *Biotechnology Progress*, 23(1) pp. 194-199.
- [64] Smay, J. E., Cesarano, J., and Lewis, J. A., 2002, "Colloidal Inks for Directed Assembly of 3-D Periodic Structures," *Langmuir*, 18(14) pp. 5429-5437.
- [65] Li, M., Tian, X., Schreyer, D. J., 2011, "Effect of Needle Geometry on Flow Rate and Cell Damage in the dispensing-based Biofabrication Process," *Biotechnology Progress*, 27(6) pp. 1777-1784.
- [66] Lewis, J. A., 2000, "Colloidal Processing of Ceramics," *Journal of the American Ceramic Society*, 83(10) pp. 2341-2359.
- [67] Smay, J. E., Gratson, G. M., Shepherd, R. F., 2002, "Directed Colloidal Assembly of 3D Periodic Structures," *Advanced Materials*, 14(18) pp. 1279-1283.
- [68] Malda, J., Visser, J., Melchels, F. P., 2013, "25th Anniversary Article: Engineering Hydrogels for Biofabrication," *Advanced Materials*, 25(36) pp. 5011-5028.
- [69] Martanto, W., Baisch, S. M., Costner, E. A., 2005, "Fluid Dynamics in Conically Tapered Microneedles," *AIChE Journal*, 51(6) pp. 1599-1607.
- [70] Xu, M., and Lewis, J. A., 2007, "Phase Behavior and Rheological Properties of Polyamine-Rich Complexes for Direct-Write Assembly," *Langmuir*, 23(25) pp. 12752-12759.
- [71] Bruneaux, J., Theriault, D., and Heuzey, M., 2008, "Micro-Extrusion of Organic Inks for Direct-Write Assembly," *Journal of Micromechanics and Microengineering*, 18(11) pp. 115020.
- [72] Osti, G., Wolf, F., and Philippi, P., 2009, "Spreading of liquid drops on acrylic surfaces," *Proceedings of the 20th International Congress of Mechanical Engineering*, International Congress of Mechanical Engineering, Gramado, RS, Brazil.
- [73] Chang, B., Nave, G., and Jung, S., 2012, "Drop Formation from a Wettable Nozzle," *Communications in Nonlinear Science and Numerical Simulation*, 17(5) pp. 2045-2051.
- [74] Wang, Y., 2016, "Capillarity and Wetting of Non-Newtonian Droplets. Available at: <http://urn.Kb.se/resolve?urn=urn:Nbn:Se:Kth:Diva-184146>," .
- [75] Duez, C., Ybert, C., Clanet, C., 2009, "Beating the Teapot Effect," *ArXiv Preprint arXiv:0910.3306*, .
- [76] Vozzi, G., Previti, A., De Rossi, D., 2002, "Microsyringe-Based Deposition of Two-Dimensional and Three-Dimensional Polymer Scaffolds with a Well-Defined Geometry for Application to Tissue Engineering," *Tissue Engineering*, 8(6) pp. 1089-1098.
- [77] Kim, J. H., Chang, W. S., Kim, D., 2015, "3D Printing of Reduced Graphene Oxide Nanowires," *Advanced Materials*, 27(1) pp. 157-161.
- [78] Kim, J. T., Seol, S. K., Pyo, J., 2011, "Three-Dimensional Writing of Conducting Polymer Nanowire Arrays by Meniscus-Guided Polymerization," *Advanced Materials*, 23(17) pp. 1968-1970.
- [79] Fuchs, N.A., 1959, "Evaporation and droplet growth in gaseous media," Pergamon Press, London; New York.
- [80] BIRDI, K., VU, D., and WINTER, A., 1989, "A STUDY OF THE EVAPORATION RATES OF SMALL WATER DROPS PLACED ON A SOLID-SURFACE," *JOURNAL OF PHYSICAL CHEMISTRY*, 93(9) pp. 3702-3703.
- [81] Hu, H., and Larson, R. G., 2002, "Evaporation of a Sessile Droplet on a Substrate," *The Journal of Physical Chemistry B*, 106(6) pp. 1334-1344.
- [82] Jin, Y., Compaan, A., Bhattacharjee, T., 2016, "Granular Gel Support-Enabled Extrusion of Three-Dimensional Alginate and Cellular Structures," *Biofabrication*, 8(2) pp. 025016.
- [83] Li, B., Clark, P. A., and Church, K., 2007, "Robust direct-write dispensing tool and solutions for micro/meso-scale manufacturing and packaging," *ASME 2007 International Manufacturing Science and Engineering Conference*, Anonymous American Society of Mechanical Engineers, pp. 715-721.
- [84] Stanley, M., 1995, "Modeling Axisymmetric Flows Dynamics of Films, Jets, and Drops," Academic Press, San Diego.
- [85] Bos, F., Wolfs, R., Ahmed, Z., 2016, "Additive Manufacturing of Concrete in Construction: Potentials and Challenges of 3D Concrete Printing," *Virtual and Physical Prototyping*, 11(3) pp. 209-225.
- [86] Jin, Y., Zhao, Z., Danyang, and Huang, Y., 2018, "Study of Extrudability and Standoff Distance Effect during Nanoclay-Enabled Direct Printing," 1(2) pp. 123-134.

- [87] Ahn, B. Y., Walker, S. B., Slimmer, S. C., 2011, "Planar and Three-Dimensional Printing of Conductive Inks," *Journal of Visualized Experiments: JoVE*, (58). pii: 3189. doi(58) pp. 10.3791/3189.
- [88] Kirby, B.J., 2010, "Micro-and Naonoscale Fluid Mechanics: Transport in Microfluidic Devices," Cambridge University Press, United States of America.
- [89] He, Y., Yang, F., Zhao, H., 2016, "Research on the Printability of Hydrogels in 3D Bioprinting," *SCIENTIFIC REPORTS*, 6pp. 29977.
- [90] Landau L., L. B., 1942, "Dragging of a Liquid by a Mvoing Plate," *Acta Physicochimica U.R.S.S.*, 17(42) pp. 42-54.
- [91] Le Berre, M., Chen, Y., and Baigl, D., 2009, "From Convective Assembly to Landau– Levich Deposition of Multilayered Phospholipid Films of Controlled Thickness," *Langmuir*, 25(5) pp. 2554-2557.
- [92] Janneck, R., Vercesi, F., Heremans, P., 2016, "Predictive Model for the Meniscus-Guided Coating of High-Quality Organic Single-Crystalline Thin Films," *Advanced Materials*, 28(36) pp. 8007-8013.
- [93] Crockett, R. S., 1997, "The Liquid-to-Solid Transition in Stereodeposition Techniques," .
- [94] McKinley, G.H., 2005, "Visco-Elasto-Capillary Thinning and Break-Up of Complex Fluids," Massachusetts Institute of Technology, USA.
- [95] Tuladhar, T., and Mackley, M., 2008, "Filament Stretching Rheometry and Break-Up Behaviour of Low Viscosity Polymer Solutions and Inkjet Fluids," *Journal of Non-Newtonian Fluid Mechanics*, 148(1-3) pp. 97-108.
- [96] Kinloch, A., 2012, "Adhesion and adhesives: science and technology," Springer Science & Business Media.
- [97] Bonn, D., Eggers, J., Indekeu, J., 2009, "Wetting and Spreading," *Reviews of Modern Physics*, 81(2) pp. 739.
- [98] Liang, T., Sun, W., Wang, L., 1996, "Effect of Surface Energies on Screen Printing Resolution," *IEEE Transactions on Components, Packaging, and Manufacturing Technology: Part B*, 19(2) pp. 423-426.
- [99] Zhou, W., 2015, "Lattice Boltzmann Simulation of Coalescence of Multiple Droplets on Nonideal Surfaces," *PHYSICAL REVIEW E*, 92(5) pp. 053307.
- [100] TII, J. C., and Baer, T. A., 1997, "Recent developments in freeform fabrication of dense ceramics from slurry deposition," *Solid Freeform Fabrication Symposium Proceedings*, Anonymous pp. 25-32.
- [101] Boley, J. W., White, E. L., Chiu, G. T., 2014, "Direct Writing of Gallium-Indium Alloy for Stretchable Electronics," *Advanced Functional Materials*, 24(23) pp. 3501-3507.
- [102] Zhou, W., List, F. A., Duty, C. E., 2016, "Fabrication of Conductive Paths on a Fused Deposition Modeling Substrate using Inkjet Deposition," *Rapid Prototyping Journal*, 22(1) pp. 77-86.
- [103] Boley, J. W., White, E. L., Chiu, G. T., 2014, "Direct Writing of Gallium-Indium Alloy for Stretchable Electronics," *Advanced Functional Materials*, 24(23) pp. 3501-3507.
- [104] Perez, K. B., and Williams, C. B., 2014, "Characterization of in-Situ Conductive Paste Extrusion on Polyjet Substrates," *International Solid Freeform Fabrication Symposium*, .
- [105] Gross, G. W., Rhoades, B. K., Azzazy, H. M. E., 1995, "The use of Neuronal Networks on Multielectrode Arrays as Biosensors," *Biosensors and Bioelectronics*, 10(6) pp. 553-567.
- [106] Mrksich, M., Dike, L. E., Tien, J., 1997, "Using Microcontact Printing to Pattern the Attachment of Mammalian Cells to Self-Assembled Monolayers of Alkanethiolates on Transparent Films of Gold and Silver," *Experimental Cell Research*, 235(2) pp. 305-313.
- [107] Palchesko, R. N., Zhang, L., Sun, Y., 2012, "Development of Polydimethylsiloxane Substrates with Tunable Elastic Modulus to Study Cell Mechanobiology in Muscle and Nerve," *Plos One*, 7(12) pp. e51499.
- [108] Muth, J. T., Vogt, D. M., Truby, R. L., 2014, "3D Printing: Embedded 3D Printing of Strain Sensors within Highly Stretchable Elastomers (*Adv. Mater.* 36/2014)," *Advanced Materials*, 26(36) pp. 6202-6202.
- [109] Hinton, T. J., Jallerat, Q., Palchesko, R. N., 2015, "Three-Dimensional Printing of Complex Biological Structures by Freeform Reversible Embedding of Suspended Hydrogels," *Science Advances*, 1(9) .
- [110] *Structur3D Prining*, 2017, "<https://www.estructur3d.io/#discov3ry>," .
- [111] Comina, G., Suska, A., and Filippini, D., 2014, "PDMS Lab-on-a-Chip Fabrication using 3D Printed Templates," *Lab on a Chip*, 14(2) pp. 424-430.
- [112] Schneider, F., Draheirn, J., Kamberger, R., 2009, "Process and Material Properties of Polydimethylsiloxane (PDMS) for Optical MEMS," *Sensors and Actuators A-Physical*, 151(2) pp. 95-99.
- [113] Robinson, A., Minev, I., Graz, I., 2011, "Microstructured Silicone Substrate for Printable and Stretchable Metallic Films," *Langmuir*, 27(8) pp. 4279-4284.